Research Square

Preprints are preliminary reports that have not undergone peer review.
They should not be considered conclusive, used to inform clinical practice,
or referenced by the media as validated information.

# Secondary Consolidation: A Novel Approach to an Old Problem

**Eduardo Rojas**

erg@uaq.mx

Universidad Autónoma de Querétaro, Centro Universitario

**Hiram Arroyo**

Universidad de Guanjuato

**Gustavo Gallegos**

Universidad Autónoma de San Luis Potosí

**Research Article**

**Keywords:** primary and secondary consolidation, Poiseuille equation, porous model, soil-water retention curves, pore size distribution

**Posted Date:** July 1st, 2026

**DOI:** https://doi.org/10.21203/rs.3.rs-10092543/v1

**License:** This work is licensed under a Creative Commons Attribution 4.0 International License.
Read Full License

**Additional Declarations:** No competing interests reported.

# SECONDARY CONSOLIDATION: A NOVEL APPROACH TO AN OLD PROBLEM

Eduardo Rojas[1], Hiram Arroyo[2] and Gustavo Gallegos[3]

[1] Ph.D., Facultad de Ingeniería, Universidad Autónoma de Querétaro, Centro Universitario, Cerro de las Campanas, CP 76010, Querétaro, Qro., México. email: erg@uaq.mx (Corresponding author)

[2] Ph.D., Universidad de Guanjuato, Campus Celaya-Salvatierra, Av. Ing. Barros Sierra No 201, CP 38140, Celaya, Guanajuato, México. email: h.arroyo@ugto.mx.

[3] Ph.D., Unidad Académica Multidisciplinaria Zona Media, Universidad Autónoma de San Luis Potosí, carretera Rio Verde-San Ciro Km 4, CP 79615, SLP, México. email: gfonseca@uaslp.mx

ABSTRACT. Generally, two causes are considered to be behind the phenomenon of secondary consolidation: the presence of micropores and the viscosity of the adsorbed water layer. In this research, Poiseuille's equation is used to establish the velocity of the flow of water during consolidation as a function of both the size of the pore and the viscosity of the fluid. In addition, a porous model based on the pore size distribution is used to analyze the water flow through the pores of soils. Using this approach, the proportion of flow occurring through large and small pores can be established. It is found that the flow of water through the macropores generates primary consolidation while secondary consolidation appears during the flow of water through the micropores. In contrast, the effect of the viscosity of water is rather marginal. With this approach, it is possible to evaluate both primary and secondary consolidation from the pore size distribution of the soil. Some comparisons between experimental and numerical results show the adequacy of

this approach. This procedure avoids the necessity of long-term consolidation tests to determine the total settlement of structures built on clayey soils.

Keywords: primary and secondary consolidation, Poiseuille equation, porous model, soil-water retention curves, pore size distribution.

## 1. INTRODUCTION

The phenomenon of secondary consolidation has been largely studied since the last century but still, there is no general agreement on its origin. The two main causes attributed to this phenomenon are the increase in viscosity of the adsorbed water layers and the presence of micropores. These two main hypotheses have been explored by different authors. In some cases, rheological models with dashpot elastic and plastic elements have been employed (Merchant [22]; Lo [18]; Wahls [30]; Christie [10]; Wu et al. [31]; Martins and Lacerda [21], among others). In other cases, exponential equations as function of time have been used (Bjerrum [6]; Hansen [16]). Also, variable permeability (Mesri [23]) or different permeabilities for the macro and microstructure in Terzaghi's consolidation equation have been explored (Figueroa [13]; Liu and Borja [17]). Some of these models result in curves with two steps: one for primary and the other for secondary consolidation. Other approaches result in a single step with secondary consolidation occurring at large times. Tests performed by Martins [20] on a mixture of 90% kaolin and 10% Bentonite show two steps (Fig. 1). The first one for primary consolidation ends at about 20 minutes. The second, for secondary consolidation, practically ends after 23 months. Similar results were reported on an organic clay in a five-year test by Andrade [3]. The end of primary consolidation was reached at about 20 minutes while the

secondary consolidation approximately ended after 3.9 years. Similar results were obtained by Cosenza y Korosak [8] on clay from Cubzac-Les-Ponts and by Berre and Iversen [5] on marine clay with 45% clay.

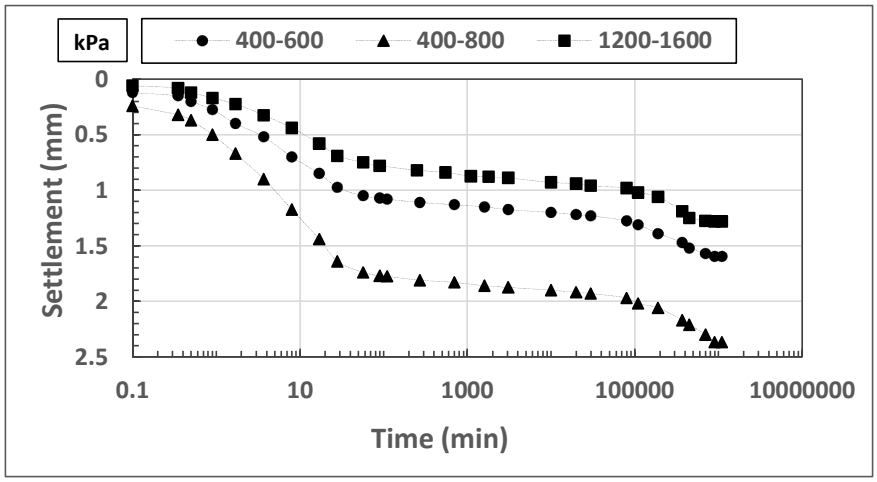



**Fig. 1** Consolidation tests at different stresses after Martins (1992)

Among the most remarkable analyses are those performed by de Josselin de Jong [11], Figueroa [13], and Liu and Borja [17]. De Josselin de Jong [11] proposed a probabilistic porous model formed by cavities and bonds or channels of different sizes where the smaller pores retarded the flow of water. This author observed that the results of this approach are essentially similar to those obtained with rheological models. A similar porous model as the one proposed by de Josselin de Jong is employed in this paper.

The procedure followed by Figueroa [13] considers a bimodal structure of the soil. The microstructure is formed by a group of aggregates with small pores and low permeability. These aggregates are embedded in the macrostructure formed by larger particles with high permeability. Then two different values for the coefficient of consolidation are considered, one for the microstructure ($C_{vm}$) and other for the macrostructure ($C_{vM}$). In addition, the proportion between the volume of the microstructure ($V_m$) with respect to the total volume of the soil ($V_T = V_M + V_m$), where $V_M$ represents the volume of the macrostructure, is included. The results are presented as a set of master curves plotted in the axes of the degree of consolidation *versus* the logarithm of time (Fig. 2). These curves depend on two parameters: $\alpha_H = T_m/T_M$, representing the ratio of the time factors of the micro ($T_m = C_{vm}\, t/H^{*2}$) and macrostructure ($T_M = C_{vM}\, t/H^{*2}$); and $r = V_m/V_T$, representing the proportion of the volume of the microstructure with respect to the total volume of the soil. The main disadvantage of this method is that the parameters of the model can only be obtained by comparing the experimental results with the master curves. Therefore, only by performing long-term consolidation tests, these parameters can be obtained. This represents an important drawback to the practical applicability of this method.

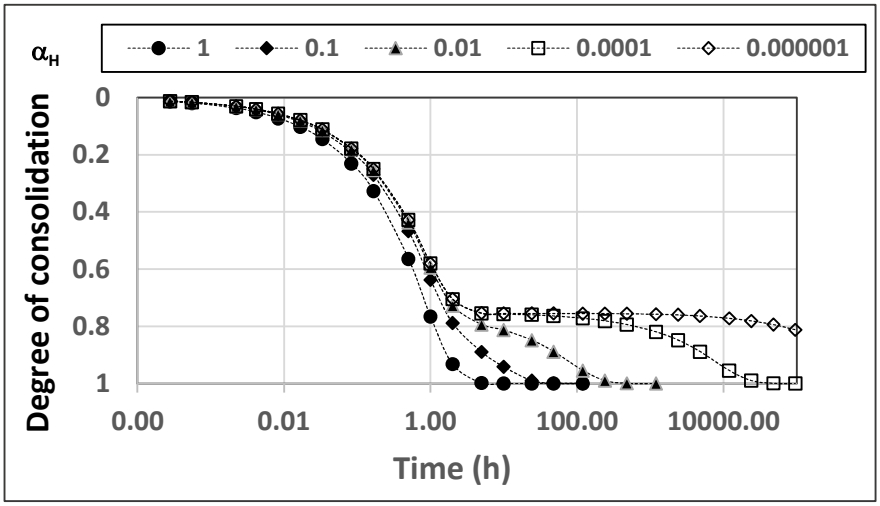



**Fig. 2** Master curves for different values of parameter $\alpha_H$ and $r$ = 0.25 (after Figueroa 1996)

Liu and Borja [17] evaluated three possible causes of secondary consolidation either individually or combined: viscoplastic behavior of the sample where a certain viscosity parameter for the soil is considered; the flow of water through macro and micropores where two different permeabilities are considered; and delayed compression due to creep as proposed by Bjerrum [6]. The first two solutions result in finite deformations for the secondary consolidation. The second solution is similar to the analysis made by Figueroa [13] and the resulting curves are also similar. The third solution results in undefined deformations for secondary consolidation similar to Bjerrum's solution which considers a constant deformation rate with time.

Regarding the results obtained from the models proposed by the different authors listed above, the doubt still subsists on which is the main cause of secondary consolidation. By adopting Poiseuille's equation for the flow of water in fine soils, it is possible to analyze the influence of both the size of

pores and the viscosity of the fluid during the phenomenon of consolidation. In addition, it is known that when soil deforms only the macropores reduce their size while the micropores remain about the same size (Simms and Yanful [27]; Yu et al. [33]). This means that the evolution of the porosimetry during loading is another factor that needs to be considered during the phenomenon of consolidation (Crawford [9]; Alexandre and Martins [1]).

The influence of the viscosity of water can be observed from the experimental results reported by Low [19]. This researcher measured the viscosity of water using three different methods with similar results (Fig.3). These methods involved the viscous flow, self-diffusion, and neutron scattering of the interlayer water. The results show that the viscosity of water for the first molecule attached to a solid increases more than 10 times the viscosity of free water. For the second to the fourth molecule, the increase is from 10 to 3 times the viscosity of free water (dotted vertical lines in Fig. 3). Considering that a pore is filled only by adsorbed water, a size of pore ranging from 0.0011 to 0.0022 μm is required to mobilize the second and fourth molecules of water, respectively. This means that both variables viscosity and small pores could be behind the phenomenon of secondary consolidation.

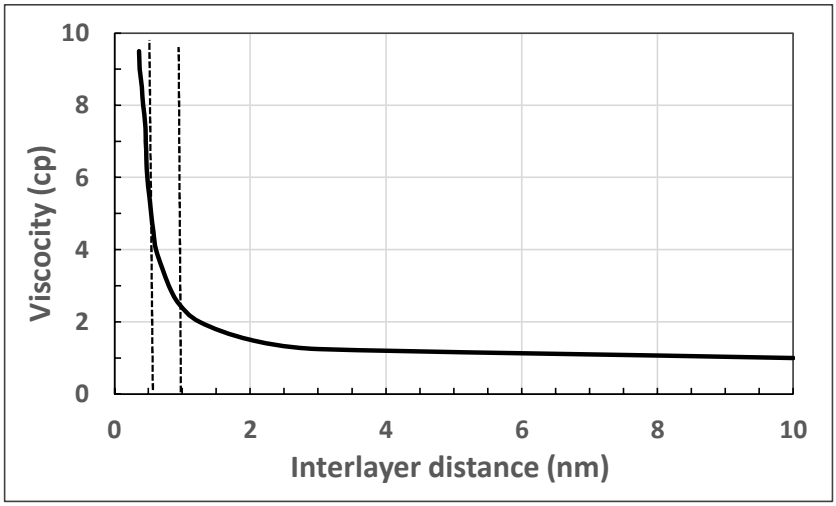



**Fig. 3** Variation of the viscosity of water with the distance to the solid particle (after Low 1979)

## 2. CONSOLIDATION EQUATION

Terzaghi's one-dimensional consolidation analysis results in a hydromechanical coupled equation for saturated materials during non-steady water flow. This equation is obtained by coupling three different equations: Terzaghi's effective stress equation, Darcy´s flow equation, and the equation for one-dimensional settlement. Terzaghi considers two assumptions for the phenomenon of consolidation: the first one establishes that solids and water are incompressible and the second one is that only the solid skeleton deforms under the action of applied stresses. In this way, the volumetric deformation of the soil results from the volume of water that flows outside the sample. In turn, the flow of water is produced by the increase in water pressure during the loading of the sample. When the resultant equation is solved through Fourier's series, the evolution of the water pressure ($u_w$) with time ($t$) and depth ($z$) can be obtained in the form

$$u_w = \Delta\sigma_v \sum_{n=0}^{\infty} \left[ \frac{2}{a} e^{-a^2 \frac{C_v t}{H^{*2}}} \sin\left(a \frac{z}{H^*}\right) \right] \quad (1)$$

where $\Delta\sigma_v$ represents the vertical increment of stress applied to the sample, $C_v$ is the coefficient of consolidation, $H^*$ is the equivalent height which depends on the drainage conditions of the sample, and $a = (2n+1)\pi/2$, with $n$ representing the summation parameter in Eq. (1). In practice, this equation is applied only for primary consolidation. In such a case, the consolidation curve is divided into primary and secondary consolidation. At the time where 50% percent of primary consolidation occurs ($t_{50}$), the coefficient of consolidation ($C_v = T_{50}\, H^{*2}/t_{50}$) is computed and the evolution of vertical displacements with time can be obtained. This procedure ensures that the computed displacements approach the experimental results. In the following sections, the same hypotheses as Terzaghi´s one-dimensional consolidation equation are assumed.

## 3. FLOW OF WATER IN FINE SOILS

In the case of fine soils, the flow of water is better represented by Poiseuille's regime. In such a case, the pores of the soil are initially considered as a bundle of capillary tubes of different sizes. Later this model is extended to the case of a network of interconnected pores made of cavities and bonds. For this analysis, the soil is considered to be homogenous. Fig. 4 represents the pore water pressure against the height of a soil sample subjected to consolidation with drainage on the upper face. The sample is split in small sections of thickness $dz$ as shown in Fig. 4. Initially, it is considered that the pores of the soil can be represented by capillary tubes of different sizes. Considering a capillary tube

of size $R_i$ and length $dz$ inside this section, the flow rate is $q_i$ and $q_i + \frac{\partial q_i}{\partial z} dz$ in the lower and upper ends of the capillary tube. Knowing that the flow rate in capillary tubes is given by Poiseuille equation $q_i = \frac{\pi \gamma_w}{8\mu} i^* R_i^4$ where, $\gamma_w$ represents the unit weight of water, $\mu$ is the viscosity of water, $i^*$ and $R_i$ represent the hydraulic gradient and the radius of the capillary tube, respectively.

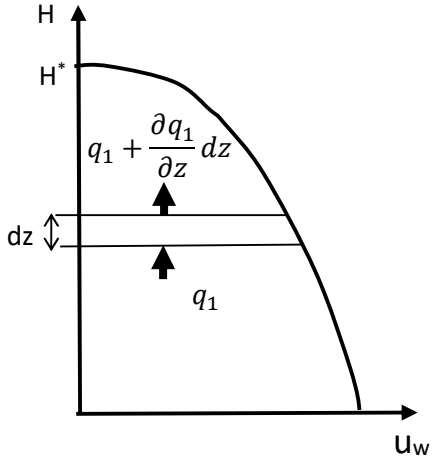



**Fig. 4** Pore water pressure profile during a consolidation process

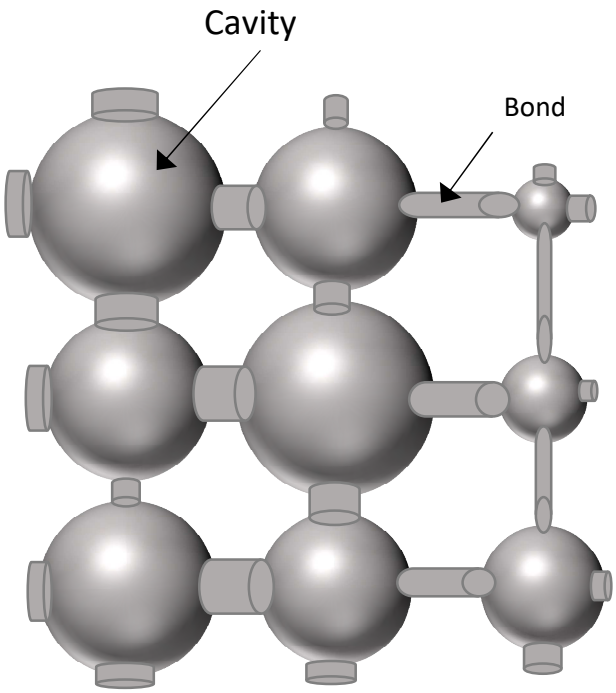
According to Fig. 4, the hydraulic gradient is given by $i^* = \frac{\partial u_w}{\gamma_w \partial z}$. Then the balance of flow can be written as $\frac{\partial q_i}{\partial z} dz = \frac{\partial}{\partial z}\left(\frac{\pi \gamma_w R_i^4}{8\mu} \frac{\partial u_w}{\gamma_w \partial z}\right) dz = \frac{\pi R_i^4}{8\mu} \frac{\partial^2 u_w}{\partial z^2} dz$, therefore, the variation of flow $dq_i$ in a capillary tube during non-steady flow is

$$dq_i = \frac{\pi R_i^4}{8\mu} \frac{\partial^2 u_w}{\partial z^2} dz \quad (2)$$

166 The term $\pi R_i^2$ represents the cross section ($A_{Bi}$) of the tube. Then the volume of drained water
167 through the capillary is
168
169 $$dV_{wi} = \frac{A_{Bi} R_i^2}{8\mu} \frac{\partial^2 u_w}{\partial z^2} dz\, dt \quad (3)$$
170
171 For a bundle of $j$ capillary tubes of different radii, the volume of drained water ($dV_{wz}$) in a section
172 with thickness $dz$ is
173
174 $$dV_{wz} = \sum_{i=1}^{j} \frac{N_{Bi}\, A_{Bi}\, R_i^2}{8\mu} \frac{\partial^2 u_w}{\partial z^2} dz\, dt \quad (4)$$
175
176 where $N_{Bi}$ represents the number of capillary tubes of size $R_i$. Real soils show a very large variation
177 in pore sizes then, the above equation can be written as
178
179 $$dV_{wz} = \sum_{R_i=0}^{\infty} \frac{A_v\, dz}{8\mu} A_{RBi}\, R_i^2 \frac{\partial^2 u_w}{\partial z^2} dt \quad (5)$$
180
181 where $A_v$ is the area of voids in a cross-section of the sample and $A_{RBi} = \frac{N_{Bi} A_{Bi}}{A_v}$ is a parameter
182 representing the relative area of all pores of size $R_i$ with respect to the total area of voids in a cross-
183 section of a homogeneous sample.
184

185 Eq. (5) holds for water flowing through straight paths however, in real soils the flow of water
186 towards the boundaries follows twisting paths which reduce the velocity of flow. These paths are
187 formed by pores of different radii going from the draining pores to the boundaries. This
188 phenomenon is called tortuosity and can be included in the above equation using the porous model
189 presented in the next section.
190
191 4. THE POROUS MODEL
192
193 The flow of water in porous media can be studied through porous models (Fatt [12], Chatzis and
194 Dullien [7]). These models intend to reproduce the porous structure of different materials. In
195 general, these models are represented by a series of interconnected pores. The pores are formed
196 by two different elements: the cavities (or sites) and the bonds (or connectors). The cavities are
197 those pores that contain most of the void volume of the porous media while the bonds connect the
198 cavities and contain a very small volume. Because several bonds converge in a single cavity, the
199 radius of the former are always smaller than those of cavities. Fig. 5 represents the arrangement of
200 cavities and bonds for a bi-dimensional regular model. In this case, the cavities are represented by
201 circles while rectangles represent the bonds. Each cavity is connected to four bonds and therefore,
202 this number represents the connectivity (C) of the network. In the case of a regular three-
203 dimensional model, the connectivity is six. In this case, cavities are represented by spheres while
204 bonds are represented by cylinders. In general, the bonds show a minimal length compared with
205 their radius, and therefore the network is highly irregular similar to real soils. Also, a variable
206 connectivity can be used to generate more realistic models. In such a case it is sufficient to consider

207 a certain percentage of bonds of size zero. Although these types of models represent the structure
208 of porous materials in a simplified manner, they have enough precision to study different aspects
209 of the flow of fluids in porous media (Chatzis and Dullien [7], Rojas et al. [25]).
210
211 Porosimetry tests indicate that most soils show a bimodal structure meaning that they have a
212 macrostructure and a microstructure (Simms and Yanful [27], [29], Yang et al. [32]). The
213 macrostructure is formed by large cavities (macrocavities) and large bonds (macrobonds) while the
214 microstructure is usually formed by aggregates with small cavities (microcavities) and small bonds
215 (microbonds). The distribution of pores sizes can be represented through logarithmic normal
216 distributions for both cavities and bonds. In the case of soils showing a bimodal structure, four
217 logarithmic normal distributions are required as they include cavities and bonds for the macro and
218 microstructure as represented in Fig. 6(a). This figure shows the PSD of a Montmorillonite clay
219 (Fleureau et al. [14]) on a plane formed by the axes of relative volume versus the logarithm of pore
220 radius.
221



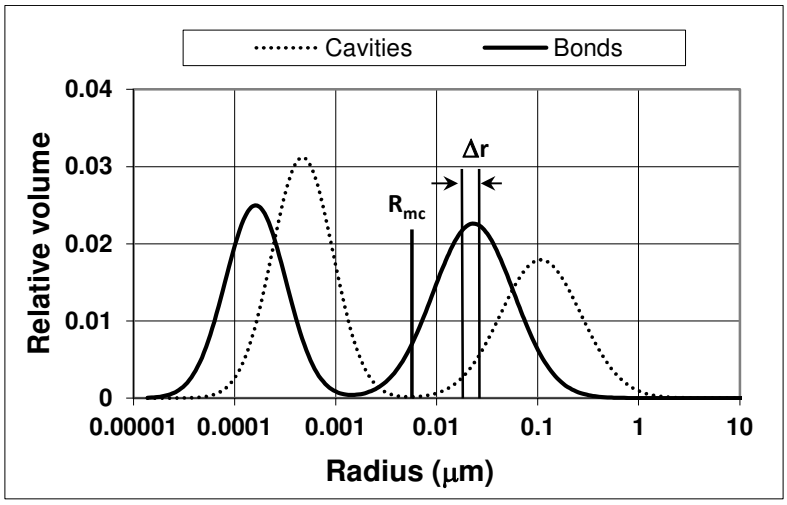

222

223 **Fig. 5** The porous model

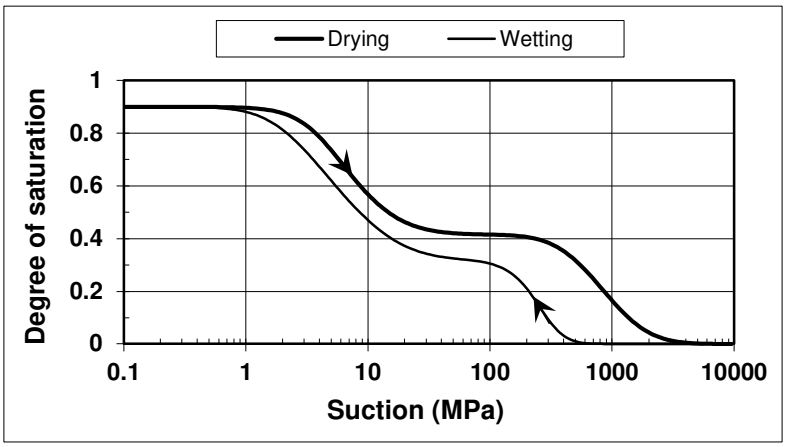
224

225 Normal distributions only require two parameters to be defined: the mean value and the standard
226 deviation. However, for double-structured soils, an additional parameter called relative volume
227 factor ($\rho_D$) is required. This parameter represents the proportion of larger pores with respect to the
228 smaller ones. Therefore, this term only affects the pore size distribution (PSD) of macropores.
229 Because there is a one-to-one relationship between the PSD and the soil-water retention curves
230 (SWRCs), it is possible to simulate the last through a porous model as proposed by different authors

231 such as Androutsopoulos [4], Simms and Yanful [28], Rostami et al. [26]. Fig. 6(b) shows the SWRCs
232 obtained from the porous model proposed herein using the PSD presented in Fig. 6(a). Because the
233 PSD of soils is not currently determined in the laboratory, it is possible to invert this process and
234 obtain the PSD by fitting the experimental SWRCs using the porous model. This approach has
235 important advantages as it is possible to establish the shift of the SSWRCs along the suction axis
236 during loading by using the current PSD of the material. The current PSD can be determined by
237 relating the relative volume factor of macropores to the plastic volumetric strain of the material as
238 established by Rojas [24].
239




240
241 (a)




(b)

**Fig. 6** (a) PSD and (b) SWRCs of a Montmorillonite clay

Because water flows easily through the largest pores, then the bonds are the elements that restrict the flow of water in soils. In addition, when an increment of stress is applied to a soil sample, only the macropores deform, reducing their size while the micropores remain mostly unaffected (Simms and Yanful [27], Yang et al. [32]). Therefore, when saturated soils are subjected to an increment in stress, the macrocavities deform and drain water through the bonds connected to these cavities. Then, other interconnected pores take this water to the boundaries. When solely continuous paths of small bonds participate in this process, slow flow occurs. In contrast, when continuous paths of large bonds take the flow of water to the boundaries, fast flow occurs. Therefore, the probability that flow occurs through paths formed by large or small bonds is a fundamental parameter to determine the volume of fast and slow flow.

Consider a cylindrical homogenous soil sample with a porous structure made of interconnected pores of different sizes. The velocity of flow depends on the size of interconnected bonds in different

directions. It is possible to determine the probability that continuous paths of small or large bonds transport water to the boundaries by making use of the porous model. This probability of flow can be established through the parameter $B^*(R_i)$ which represents the probability of a bond being smaller or equal to the size $R_i$. For a single distribution, this value is given by the relationship

$$B^*(R_i) = \int_0^{R_i} f_B(R_i)\, dR \tag{6}$$

where $f_B(R_i)$ represents the frequency of bonds of size $R_i$ in a logarithmic normal distribution as represented in Fig. 6(a). The function $f_B(R_i)$ is defined as

$$f_B(R_i) = \frac{e^{-\frac{\left(L_{Ri} - L_{\bar{R}B}\right)^2}{2L_{SB}^2}}}{\sqrt{2\pi}\, L_{SB}} \tag{7}$$

where $L_{Ri}$, $L_{\bar{R}B}$, and $L_{SB}$ represent the logarithm of the radius of a bond of size $R_i$, the logarithm of the mean radius of bonds $\bar{R}_B$, and the logarithm of the standard deviation, respectively. The above definition ensures that $\int_0^{\infty} f_B(R_i)\ dR = 1$. This means that the probability of finding pores of size $R_i$ in a network for single-structured soils is

$$dB^*(R_i) = f_B(R_i)\, dR \tag{8}$$

As stated before, for the case of double-structured soils two logarithmic normal distributions are required, one for the macro and another for the microstructure. These distributions are linked to the PSD of the material where the relative volumes for the macro and microstructure can be observed as shown in Fig 6(a). In such a case, the probability of finding a bond of size $R_i$ in the network is

$$dB(R_i) = \frac{\varrho_D \, f_B(R_i) \, dR}{B'(R_m)+B'(R_M)} \tag{9}$$

where $\varrho_D$ is the relative volume factor, and subindex $D$ represents either the macro ($M$) or the microstructure ($m$) of soil. For the microstructure $\varrho_m = 1$, while for the macrostructure $\varrho_M \neq 1$. additionally, $B'(R_M)$ and $B'(R_m)$ represent the single distributions of the macro and microbonds affected by the relative volume factor $\varrho_D$ which, according to Eq. (6), can represented by the relationship

$$B'(R_D) = \varrho_D \int_{R_i=R_n}^{R_f} f_B(R_i) \, dR \tag{10}$$

where $R_n$ and $R_f$ represent the initial and final radius for each distribution. For the microstructure $R_n = 0$, and $R_f = R_{mc}$, while for the macrostructure $R_n = R_{mc+1}$, and $R_f = \infty$, where $R_{mc}$ represents the maximum size of microbonds as shown in Fig. 6(a). Then, the distributions for the micro ($B(R_m)$) and macrobonds ($B(R_M)$) are obtained by integrating Eq. (9) between the corresponding limits of each distribution, in the form

299

300 $$B(R_D) = \int_{R_n}^{R_f} dB(R_i) = \int_{R_n}^{R_f} \frac{\varrho_D \, f_B(R_i) \, dR}{B'(R_m) + B'(R_M)} \quad (11)$$

301

302 The above equation ensures that $B(R_m) + B(R_M) = 1$. These equations are used in the following
303 section to determine the probability of finding paths for fast and slow flow.

304

305 5. CONSOLIDATION EQUATION FOR FINE SOILS

306

307 As stated before, during the compression of a saturated soil, water flows through continuous paths
308 of interconnected pores that link the contracting cavities to the boundaries of the sample. When
309 bimodal structured soils are considered, water flows at different velocities depending on the size of
310 the pores involved. If the flow of water happens through macrobonds then, fast flow occurs. On the
311 contrary, slow flow occurs when it happens through microbonds. The probability that bonds
312 participate in slow or fast flow depends on the PSD of the soil, and specifically depends on the
313 probability of finding continuous paths formed by slow or fast flow basic units as sketched in Fig. 7.
314 For the case of two-dimensional networks, the basic unit for slow flow or secondary consolidation
315 is made of one cavity connected to four microbonds as shown in Fig. 7(a). This arrangement ensures
316 that the flow of water necessarily occurs through microbonds. In addition, the basic unit for fast
317 flow or primary consolidation is formed by one cavity connected to at least one macrobond as
318 shown in Fig. 7(b). In this case, most of the flow occurs through the macrobonds.

319

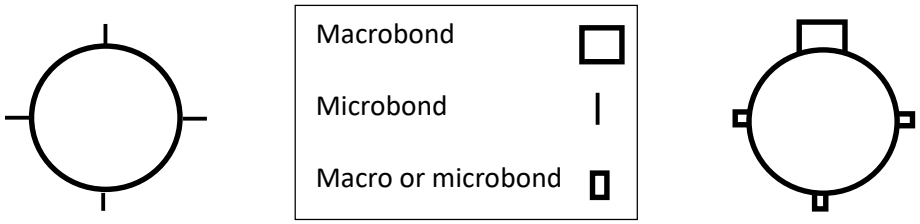



**Fig. 7** Basic units for a) fast and b) slow flow

The conditions for a microbond of size $R_i$ ($0 < R_i \leq R_{mc}$) to participate in continuous paths of slow flow units that reach the boundaries of the soil sample are: a) at least two bonds have the specific size $R_i$. This condition ensures that water flows in and out of the cavity through a bond of size $R_i$; and b) all remainder pores converging to the cavity have a size equal or smaller than $R_i$. This last condition ensures that the flow of water occurs predominantly trough pores of size $R_i$. The first condition is represented by the term $dB(R_i)^2$ as establish by Eq. (9). The second condition is represented by the term $B(R_i)^{C-2}$, where $B(R_i)$ is represented by the integral of Eq. (9), in the form $B(R_i) = \int_0^{R_i} dB(R_i) = \int_0^{R_i} \frac{\varrho_D \, f_B(R_i) \, dR}{B'(R_m)+B'(R_M)}$. Therefore, the probability that microbonds of size $R_i$ participate in the process of secondary consolidation ($P_m(R_i)$ is represented by the product of the two above conditions, as they must occur simultaneously

$$P_m(R_i) = B(R_i)^{C-2} dB(R_i)^2 \tag{12}$$

Then, the probability to find continuous paths of microbonds of any size is $P_{mc} = \int_0^{R_m} \int_0^{R_m} B(R_i)^{C-2} dB(R_i) \, dB(R_i) = B(R_m)^C$, where $B(R_m)$ is given by Eq. (11), with $R_n = 0$, and $R_f = R_{mc}$. Then, $P_{mc}$ accounts for the tortuosity of flow during secondary consolidation.

In addition, the condition for a bond of size $R_i$ to participate in continuous paths of fast flow units ($(P_M(R_i))$) is represented by any combination of bonds except that given by Eq. (12), and can be written as

$$P_M(R_i) = B(R_i)^{C-1} dB(R_i) - P_m(R_i) \tag{13}$$

with $0 < R_i < \infty$. Then the tortuosity factor for primary consolidation is $P_{Mc} = B(R_\infty)^C - B(R_m)^C = 1 - B(R_m)^C$, where $B(R_\infty) = \int_0^\infty dB(R_i) = 1$. Observe that the addition of Eqs. (12) and (13) for the full range of bonds becomes one, meaning that all possible combinations of flow are covered with these two equations. Therefore, depending on the size of the analyzed bond, there is a certain probability that this bond participates in primary or secondary consolidation. This probability of flow dependent on the size of pores affects Eq. (5) because it is written precisely in terms of the size of the pore $R_i$. Therefore, Eq. (5) transforms into

$$dV_{wz} = \sum_{R_i=0}^{\infty} \frac{A_v\, dz}{8\mu} A_{RB_i} \left[P_M(R_i) + P_m(R_i)\right] R_i^2 \frac{\partial^2 u_{wi}}{\partial z^2}\, dt \tag{14}$$

where the term $P_m(R_i)$ only applies in the range $0 < R_i \leq R_m$, while $P_M(R_i)$ applies for the full range of bonds. The inclusion of these terms modifies the velocity of flow due to the phenomenon of tortuosity and depends on the size of the analyzed pore.

In addition, the term $A_{RB_i}$ depends on the number of bonds ($N_{Bi}$) of the specific size ($R_i$) in a cross-section of the sample. The value of $N_{Bi}$ can be obtained from the relationship

$$N_{Bi} = N_B \, f_B(R_i) \, \Delta R \tag{15}$$

where $N_B$ represents the total number of bonds and $\Delta R$ is the increment in the size of pores used to divide the PSD into different sections as represented in Fig. 6(a). The number of bonds depends on the size and connectivity of the porous network. Moreover, in a cross-section of the sample, the area of voids ($A_v$) is obtained from the addition of the area of all cavities and bonds of the section. This value is given by the term

$$A_v = \sum_{R_i=0}^{\infty} \left( N_{Ci} \, A_{Ci}(R_i) + N_{Bi} \, A_{Bi}(R_i) \right) \tag{16}$$

where $A_{Ci}(R_i)$ and $A_{Bi}(R_i)$ represent the areas of a single cavity and bond of size $R_i$, respectively, and $N_{Ci}$ is the number of cavities of size $R_i$. Parameter $N_{Ci}$ is defined similarly as $N_{Bi}$ in Eq. (15)

$$N_{ci} = N_C \, f_C(R_i) \, \Delta R \tag{17}$$

where $N_C$ represents the number of cavities in the network and $f_C(R_i)$ is the frequency of cavities of size $R_i$. Parameter $f_C(R_i)$ is defined similarly as Eq. (7) using the logarithms of the mean size $L_{\bar{R}C}$ and standard deviation $L_{SC}$ for cavities. Then, the relative area of bonds $A_{RBi}$ of size $R_i$ with respect to the total area of voids can be written as

386

387 $$A_{RBi} = \frac{N_{Bi}\, A_{Bi}}{A_v} = \frac{N_{Bi}\, A_{Bi}(R_i)}{\sum_{R_i=0}^{\infty}[N_{Ci}\, A_{Ci}(R_i)+N_{Bi}\, A_{Bi}(R_i)]} \quad (18)$$

388

389 When the dimension and the size of the network are defined, then it is possible to compute the
390 number of cavities $N_C$ and bonds $N_B$ to finally obtain the value of parameter $A_{RBi}$ which is used in
391 Eq. (14) to quantify the volume of water that flows through a section during certain time.

392

393 Furthermore, the variation in volume ($dV_{mz}$) of a section of soil with thickness $dz$ produced by the
394 drainage of water can be obtained from the equation for vertical deformation multiplied by the
395 cross-section of the sample $A_m$, in the form

396

397 $$dV_{mz} = -\frac{a_v}{1+e_0} du_w A_m dz \quad (19)$$

398

399 where $a_v$ represents the coefficient of compressibility of the soil. The disadvantage of the use of
400 parameter $a_v$ in the above equation is that its value depends on the current stress applied to the
401 sample. However, it can be related to the elastoplastic compression index $\lambda_e$ which remains
402 constant for stresses above the preconsolidation stress. Considering that the elastoplastic
403 compression of soils can be represented by a straight line in a logarithmic plane formed by the axes
404 of void ratio and vertical stress, the following relationship between the current vertical stress ($\sigma_v$)
405 and void ratio ($e$) can be written (Rojas [24])

406

$$\frac{e}{e_0} = \left(\frac{\sigma_v}{\sigma_{v0}}\right)^{\lambda_e} \quad (20)$$

where $\sigma_{v0}$ and $e_0$ represent the vertical stress and void ratio before the new increment of stress has been applied, respectively. The derivative of the above equation writes

$$de = \lambda_e \frac{e}{\sigma_v} d\sigma_v \quad (21)$$

and because $a_v = de/d\sigma_v$, it results that

$$a_v = \lambda_e \frac{e}{\sigma_v} \quad (22)$$

Then Eq. (19) can be written as

$$dV_{mz} = -\lambda_e \frac{e\, A_m dz}{\sigma_v\,(1+e_0)} du_w \quad (23)$$

By equating Eqs. (14) and (23) and considering soil as a homogenous material such that $\frac{A_m\, dz}{A_v\, dz} = \frac{1+e_0}{e}$, the consolidation equation becomes

$$\sum_{R_i=0}^{\infty} \left\{\frac{\sigma_v}{8\mu\, \lambda_e} A_{RB_i} \left[P_M(R_i) + P_m(R_i)\right] R_i^2\right\} \frac{d^2 u_w}{dz^2} = -\frac{du_w}{dt} \quad (24)$$

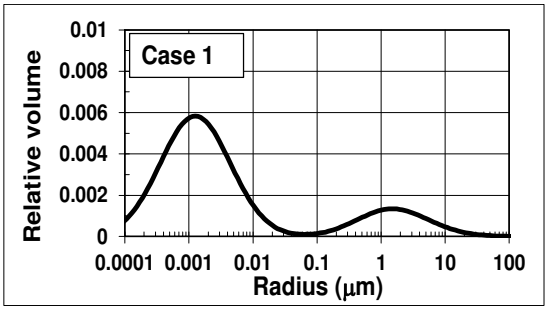
427 This relationship is similar to Terzaghi's consolidation equation except that the coefficient of
428 consolidation $C_{vi} = \frac{\sigma_v}{8\mu\,\lambda_e} A_{RB_i}\,[P_M(R_i) + P_m(R_i)]\,R_i^2$ takes different values depending on the size
429 of the pore $R_i$ and the current effective stress. Therefore, the pore water pressure at a certain depth
430 ($z$) and time ($t$) produced by an increment of vertical stress $\Delta\sigma_v$, can be determined from Terzaghi's
431 original solution (Eq. (1)). Accordingly, the pore water pressure $u_{wi}$ for a certain $C_{vi}$ at a certain
432 depth $z$ and time $t$, is given by the relationship
433
434 $$u_{wi} = \Delta\sigma_v \sum_{n=0}^{\infty} \left[\frac{2}{a} e^{-a^2 \frac{C_{vi}\,t}{H^{*2}}} \sin\left(a\,\frac{z}{H^*}\right)\right] \tag{25}$$
435
436 The pore water pressure as established in Eq. (25) depends on the size distribution of bonds through
437 the parameter $C_{vi}$. This effect also appears when the soil is considered as a heterogeneous material
438 formed by a matrix with aggregates showing different permeabilities as considered by Figueroa [13],
439 and Liu and Borja [17], although in these cases only two different $C_{vi}$ are considered.
440
441 The weighted mean pore water pressure at the center of a section located at depth $z$ and formed
442 by pores of different sizes can be determined with the relationship $u_{wz} = \sum_{R_i=0}^{\infty} u_{wi}\,dB(R_i)$. Then,
443 the variation in the void ratio ($de_z$) for one section of the soil is obtained from Eq. (21) written in
444 the form
445
446 $$de_z = -\lambda_e \frac{e}{\sigma_v} \sum_{R_i=0}^{\infty} (u_{w0} - u_{wi})\,dB(R_i) \tag{26}$$
447

448 where $u_{w0}$ and $u_{wi}$ are the initial pore water pressure (equal to $\Delta\sigma_v$ ), and the pore water pressure
449 obtained from Eq. (25). According to Eq. (24), soils with a small microstructure show a small
450 deformation during secondary consolidation. On the contrary, soils with an important
451 microstructure produce large deformations during secondary consolidation. If the material is loaded
452 below the preconsolidation stress then, the elastic compressibility index $k_e$ replaces $\lambda_e$. The
453 introduction of the compression index instead of the coefficient of compressibility in Eq. (22), makes
454 this approach more practical. Finally, the reduction in the mean size of macropores during
455 consecutive loading in the consolidation process can be included in the porous model through
456 parameter $\varrho_M$ to better simulate the experimental results. It can be established that during
457 consecutive loading, macropores reduce in size and therefore, the volumetric deformation for
458 primary consolidation also reduces.
459
460 In summary, to simulate the consolidation process, the soil sample is divided into small sections with
461 the same thickness, and the time is increased by steps, each time step doubles the previous. Also,
462 the size distribution curve for bonds is divided into sections of the same thickness and the mean size
463 of bonds for each section is established. Subsequently, the coefficient of consolidation is computed
464 for each range of sizes and the pore water pressure for each coefficient of consolidation is obtained.
465 Then, the change in void ratio for each section is computed and added to finally obtain the variation
466 in void ratio of the whole sample at certain time. To achieve this process, the following data are
467 required: the PSD of bonds, both the elastic and elastoplastic compression indexes, the initial void
468 ratio, the increment of vertical stress, the current vertical stress, and the preconsolidation stress.
469 Because the size distribution of bonds in most porosimetry techniques is rather elusive because of

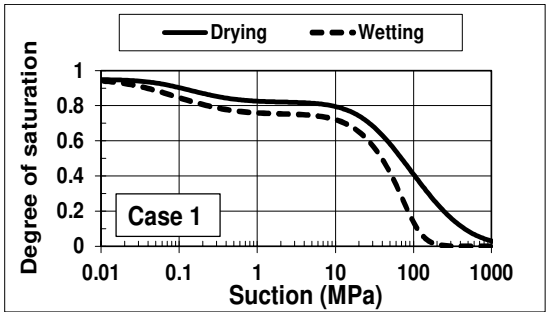
470 the small volume contained by these elements compared with that of cavities, it is convenient to
471 use an alternative procedure. In that sense, it is possible to obtain the PSD for bonds and cavities
472 of the material by fitting the experimental SWRCs at wetting and drying, with the numerical curves
473 obtained from the porous model described before. To this purpose, an initially proposed PSD is
474 successively modified until the best fit with the experimental SWRCs is obtained (Rojas [24]). The
475 experimental SWRC must be determined at the initial void ratio of the soil sample.
476
477 Fig. 8 shows some simulations of consolidation tests made for six different materials using the
478 procedure outlined above. The PSDs of the different cases (1 to 6) are shown in figures (a), the
479 SWRCs in figures (b), and the variations on void ratio with time is shown in figures (c). For these
480 materials, all parameters remain constant except the initial PSD. The initial height of the sample is
481 $H$ = 2 cm and it is drained at both ends ($H^*$= 1). The initial void ratio of the sample is $e_0$ = 0.82 with
482 an initial stress of $\sigma_{v0}$= 0.01 MPa which is equal to the preconsolidation stress. The elastoplastic
483 compression index is $\lambda_e$= 0.16 and the increment of stress is $\Delta\sigma_v$= 0.25 MPa. For the first case, a
484 large microstructure and small macrostructure with a standard deviation of 3.5 for both elements
485 is considered (Fig. 8(1a)). The retention curves show a small section for low values of suction
486 produced by the macrostructure while most of the curve appears for suctions larger than 10 MPa
487 and is produced by the microstructure (Fig. 8(1b)). For this case, the consolidation curve shows two
488 steps: a small one for primary consolidation and a large one for secondary consolidation starting
489 about 5 days after the load increment is applied (Fig. 8(1c). The PSD of sample 2 shows a standard
490 deviation of 1.1 for the microstructure and 3.5 for the macrostructure (Fig. 8(2a)) which is now the
491 major proportion of soil. This PSD results in a retention curve that develops mostly for suctions

below 1 MPa (Fig. 8(2b)). In this case, the consolidation curve shows a large primary consolidation that ends at about 5 min then a large period of very small deformations followed by a small step for secondary consolidation starting at about 6 months after the loading (Fig. 8(2c)). For sample 3, the PSD shows a large proportion of microstructure with a standard deviation of 1.5 and 3.5 for the macrostructure (Fig. 8(3a)). The SWRC develops mostly in the range of suction above 10 MPa (Fig. 8(3b)). In this case, the secondary consolidation shows a large step that starts about 3 months after the loading (Fig. 8(3c)). Sample 4 shows the same standard deviations of 3.5 for both the micro and macrostructure but with a small proportion in the microstructure (Fig. 8(4a)). In this case, primary consolidation is predominant with a small secondary consolidation starting about 20 days after the loading (Fig. 8(4c)). In cases 1 to 4 no overlap occurs in the PSD between the macro and microstructure. In contrast, the PSD of case 5 shows an important overlap between the macro and the microstructure with a standard deviation of 3.5 for the macro and 2.5 for the microstructure (Fig. 8(5a)). The SWRC shows a shape similar to single-structured soils with small variations in the degree of saturation for small values of suction (Fig. 8(5b)). The microstructure represents the major proportion of the soil and large secondary consolidation is expected. In this case, the consolidation curve shows a single step where it is difficult to differentiate the primary from the secondary consolidation (Fig. 8(5c)). The PSD for case 6 also shows an important overlap between the micro and the macrostructure (Fig. 8(6a)) but in this case, the macrostructure represents the major proportion of the soil. The standard deviations for the macro and the microstructure remain the same as for case 5. Similar to case 5, the consolidation curve shows a single step but, in this case, a large instant deformation is observed and no clear distinction can be made between primary and secondary consolidation (Fig. 8(6c)).

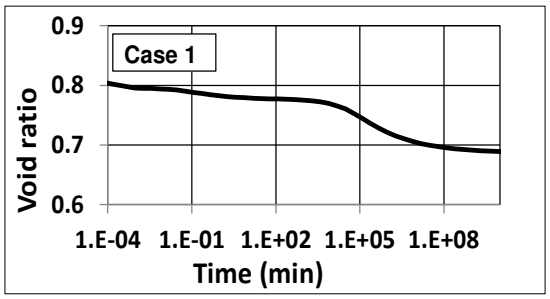
From these simulations, it can be concluded that the shape of the consolidation curve depends on the PSD which in turn defines the SWRCs of the soil. When the PSD is of the bimodal type with two well-differentiated mean sizes with no overlap, the consolidation curve shows two steps, one for primary and the other for secondary consolidation. The height and length of the step for primary and secondary consolidation depend on the proportion and standard deviation of the macro and microstructure of the soil, respectively. The mean sizes and standard deviations for the macro and microstructures define the time at which primary and secondary consolation occur, respectively. On the contrary, when the size distributions for the macro and micro structure overlap, then the consolidation curve shows a single step and the limit between primary and secondary consolidation is difficult to establish. Between these limits, different combinations of curves for the primary and secondary consolidation can be obtained. Additionally, large standard deviations in the PSD of the microstructure produces deformations with a continuous slope with respect to the logarithm of time. In fact, deformations only end at time infinity as this model is based on Terzaghi's solution.



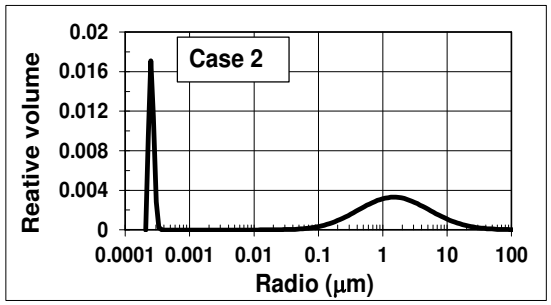

(1a)



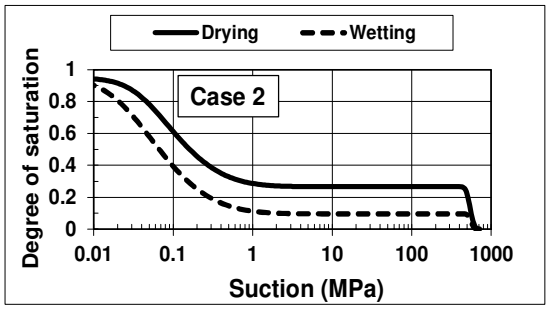

(1b)



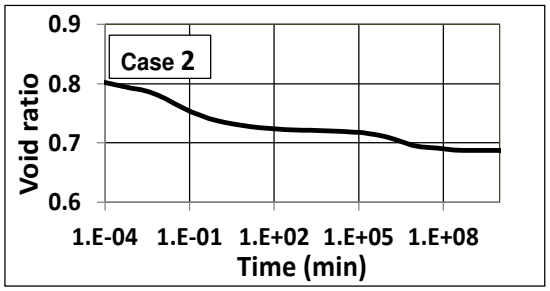

(1c)



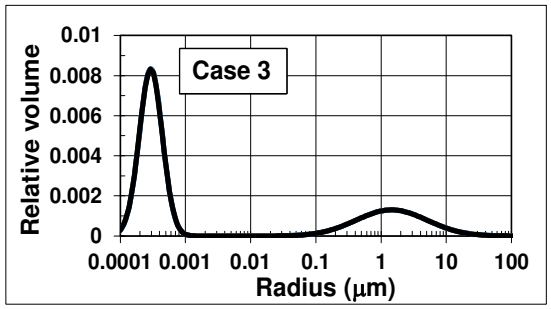

(2a)



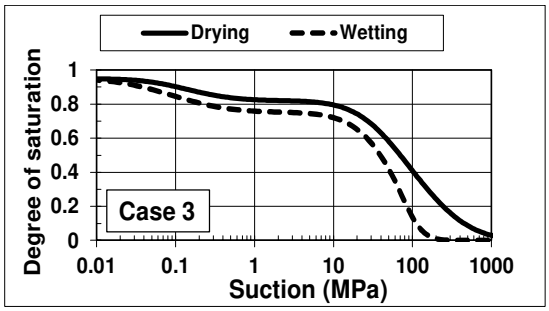

(2b)



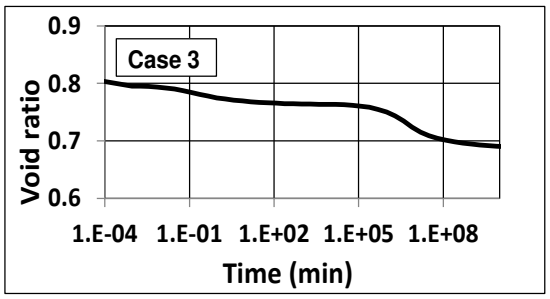

(2c)



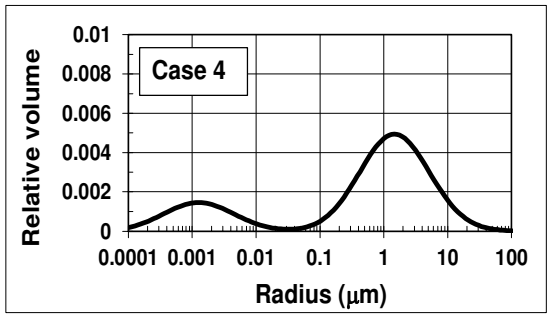

(3a)



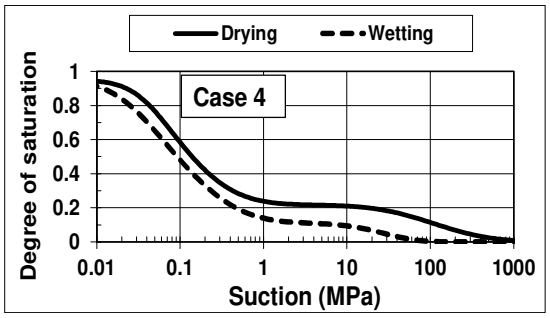

(3b)



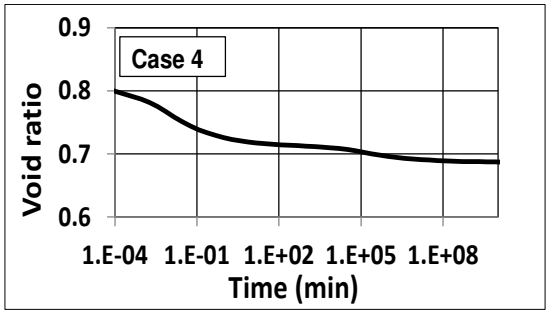

(3c)



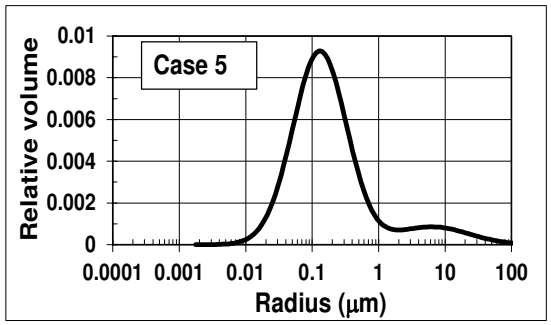

(4a)



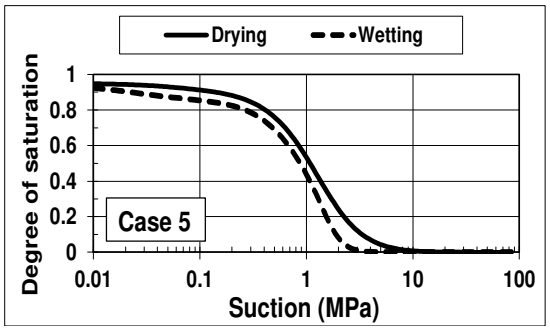

(4b)



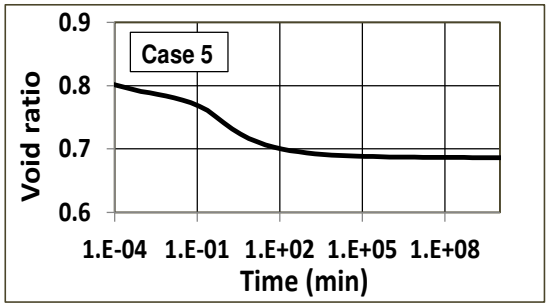

(4c)



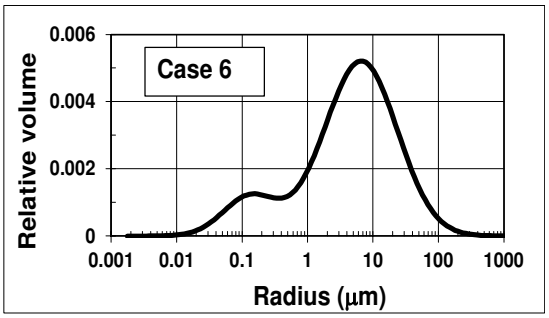

(5a)



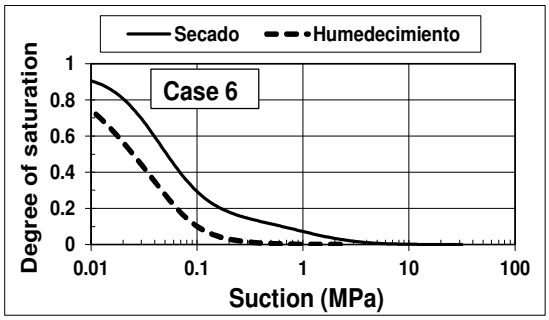

(5b)



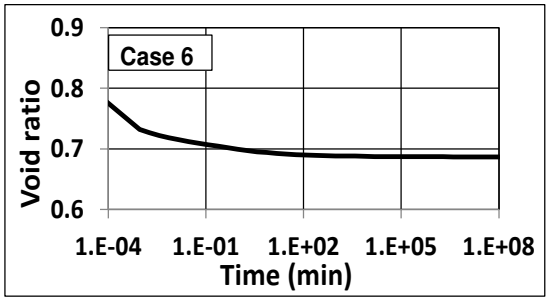

(5c)




(6a)




(6b)



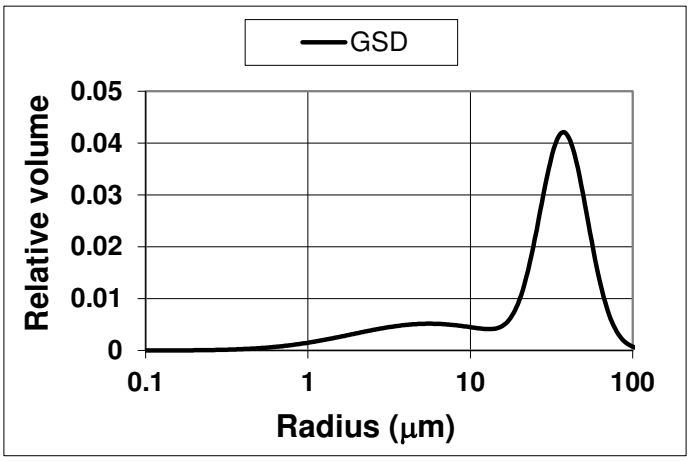

(6c)

**Fig. 8** Different cases for the (a) SWRC, (b) the PSD, and (c) consolidation curve of soils

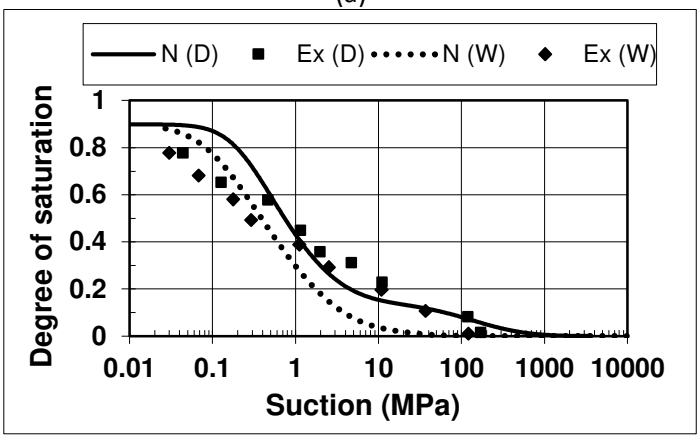
Some limitations of the proposed porous model are the following: it only considers circles and rectangles (2D), or spheres and cylinders (3D) for cavities and bonds, respectively. More realistic shapes of pores are not considered. Another point is related to the connectivity of the cavities. Although the value for connectivity ($C$) does not necessarily require an entire number, the model considers a constant connectivity ($C$) while in general, real porous media show variable connectivity.

578 This aspect can be covered by considering a certain proportion of pores of size zero. With respect
579 to the proposed consolidation equation more simulations including alternated large and small load
580 increments and different consolidation times are required to evaluate the precision of the model.
581
582 6. MATERIALS AND METHODS
583
584 A series of consolidation tests were performed using two different soils. The first one is a
585 homogeneous industrial kaolin. This material has a specific weight of solids of 2.53, a Liquid Limit
586 (LL), and Plastic Limit (PL) of 38% and 25%, respectively. The specific surface is 30 $m^2/g$, the saturated
587 permeability is 8 x $10^{-4}$ cm/s and the soil is classified as low compressibility silt (ML). Initially, the
588 material was slightly compacted at a water content of 7% in the consolidation ring. Then, it was
589 saturated by capillarity showing an important collapse during this process. The initial void ratio of
590 the sample after saturation was 0.83 while the preconsolidation stress after saturation was 0.01
591 MPa. The consolidation test was performed for an increment of stress of 0.25 MPa with an initial
592 loading of 0.01 MPa to ensure that the sample started the loading stage above the preconsolidation
593 stress. The initial height of the sample was 2 cm.
594
595 The GSD in the axes of relative volume *vs.* the radius of the particle is shown in Fig. 9(a). This curve
596 shows that all solids are finer than sieve #100, and only 33% is retained in sieve #200. The
597 experimental SWRCs and their numerical simulation using the porous model are shown in Fig. 9(b).
598 The experimental points were obtained using the filter paper method. From the simulation of these
599 curves using the porous-solid model, the numerical PSD of the material was obtained as shown in
600 Fig. 9(c). This same figure shows the experimental results of porosimetry tests using the nitrogen
601 adsorption technique. The smallest pore radius that can be measured with this method is

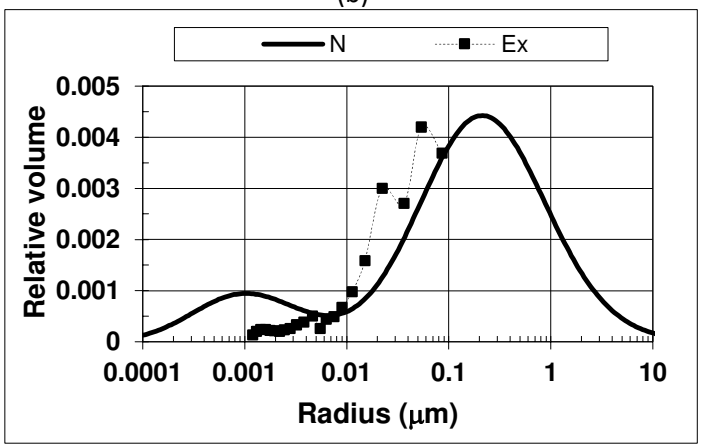
602 considered to be around 0.002 μm. However, according to Fig. 9(c) the maximum radius that can be
603 measured with this method is around 0.005 μm, which makes that the smallest pores of this material
604 cannot be detected with this method. Notice that the curves for the GSD (Fig. 9(a)) and the PSD (Fig.
605 9(c)) are quite similar as observed by Alonso et al. [2] for different soils.
606
607 Once the initial PSD of the material is obtained, it is possible to simulate the consolidation tests
608 performed on this material. The experimental and numerical results for this test are shown in Fig.
609 9(d). The experimental results show a very quick primary consolidation ending at about 6 seconds
610 after the loading while for the numerical simulation, it takes about one minute. This difference is
611 generated by the larger standard deviation of the macropores in the numerical (N) PSD when
612 compared with the experimental (Ex) PSD as observed in Fig. 9(c). The step produced by secondary
613 consolidation starts around one week after loading and practically ends after four months. The
614 numerical simulation shows a slightly larger deformation during secondary consolidation than the
615 experimental results. Because the height of the step for secondary consolidation with respect to
616 primary consolidation depends on the proportion of fines in the soil, the secondary consolidation
617 results in a small step as could be anticipated from Fig. 9(c). Notice that in Fig. 9(d) there are two
618 numerical curves: one considering the normal viscosity of free water at $20^0$ C for the adsorbed water
619 layer (v = 1, in the figure) while the second one considers a viscosity of 10 times this value (v = 10).
620 Therefore, the increase in the viscosity of water is considered only for the microstructure. In the
621 figure, it can be observed that the increase in viscosity of water reduces the velocity of the
622


GSD
Relative volume
0.05
0.04
0.03
0.02
0.01
0
0.1
1
10
100
Radius (μm)

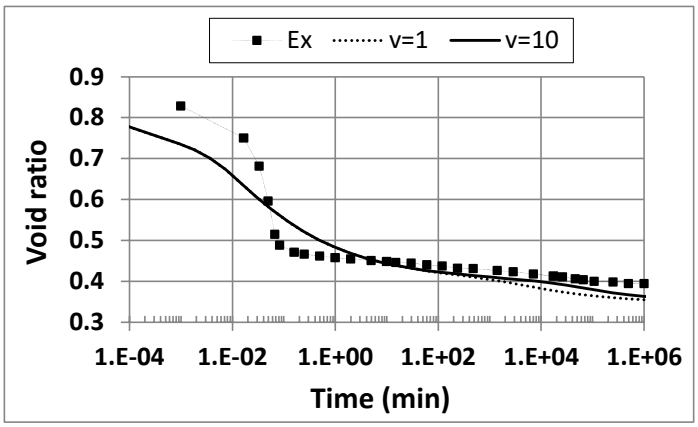
(a)


N (D)
Ex (D)
N (W)
Ex (W)
Degree of saturation
1
0.8
0.6
0.4
0.2
0
0.01
0.1
1
10
100
1000
10000
Suction (MPa)

(b)


N
Ex
Relative volume
0.005
0.004
0.003
0.002
0.001
0
0.0001
0.001
0.01
0.1
1
10
Radius (μm)

(c)



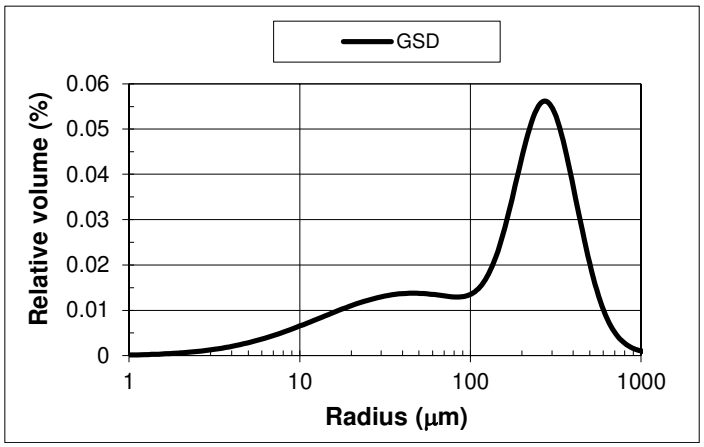

(d)

**Fig. 9** Experimental (Ex) and numerical (N) (a) GSD, (b) SWRCs, (c) PSD, and (d) consolidation test for the kaolin sample considering two different viscosities (v) for the adsorbed water layer

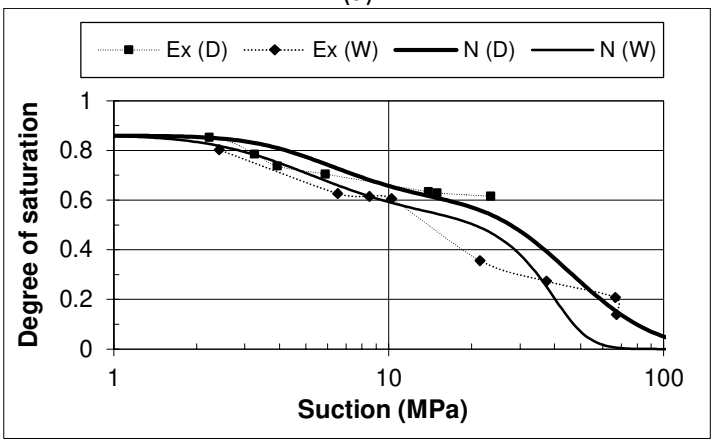
deformation of the soil during the secondary consolidation but in the end, the final deformation is the same for both cases.

The second tested material is clay from the Texcoco lake in Mexico City and was obtained at 19.5 m in depth. This material shows a specific weight of solids of 2.26, a volumetric weight of 1.15 g/cm$^3$, a LL and PL of 268% and 164%, respectively. The soil is classified as silty sand (SM). The preconsolidation stress of this material is around 0.03 MPa. It was decided to trim the sample 1 cm in height to reduce the testing time. The GSD of the material is shown in Fig. 10(a) while the experimental and numerical SWRCs at wetting and drying are shown in Fig. 10(b). Fig. 10(c) shows the experimental PSD obtained from the nitrogen adsorption technique. In this same figure, the initial numerical PSD (PSDi) obtained by fitting the SWRCs with the porous model is presented. Again, the experimental results (Ex) obtained from the nitrogen adsorption technique show a smaller proportion of micropores when compared with the numerical results. Once again, the minimum radius of pores detected by this method is around 0.005 μm. This figure also shows the final numerical PSD (PSDf) at the end of the consolidation process generated by the first increment of stress (0.25 MPa). Observe that the relative volume of micropores increases. This effect is

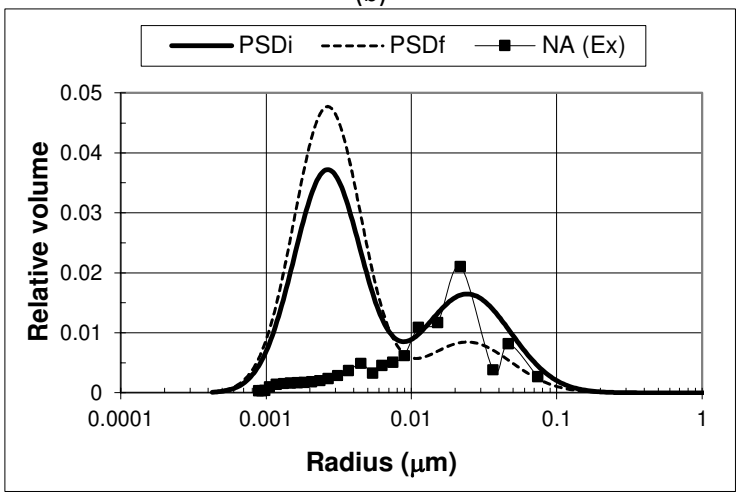
produced by the reduction of the relative volume of macropores during the consolidation process. Fig. 10(d) shows the experimental results of the consolidation test for two different increments of stress. The first increment of stress was from 0.03 to 0.25 MPa while the second was from 0.25 to 0.75 MPa. The primary consolidation for both increments of stress occurs during the first 12 seconds and overlaps with secondary consolidation which practically ends about 10 days after the loading. In the same figure, the numerical results obtained from the proposed equations are shown. Again, primary consolidation occurs faster than the numerical results predict. Observe that during the first loading, the void ratio of the sample changes from 11.5 to 8.5, and this volumetric variation modifies the PSD of the material (as shown in Fig. 10 (c)) which in turn affects the behavior of the soil during the second loading. To observe the influence in the variation of the PSD of the sample during the second loading, two numerical curves are shown. The dotted line represents the consolidation curve when the PSD of the material is updated while the continuous line was obtained using the original PSD of the material. When the variation in the PSD is considered for the second increment, the numerical results approach better the experimental points. Finally, Fig. 10(e) shows the shift of the SWRCs in the axis of suction at the end of the first loading.


GSD
Relative volume (%)
0.06
0.05
0.04
0.03
0.02
0.01
0
1
10
100
1000
Radius (μm)

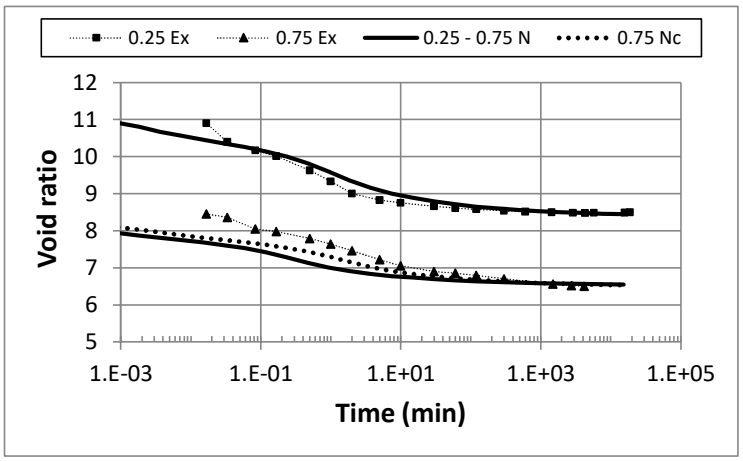
(a)


Ex (D)
Ex (W)
N (D)
N (W)
Degree of saturation
1
0.8
0.6
0.4
0.2
0
1
10
100
Suction (MPa)

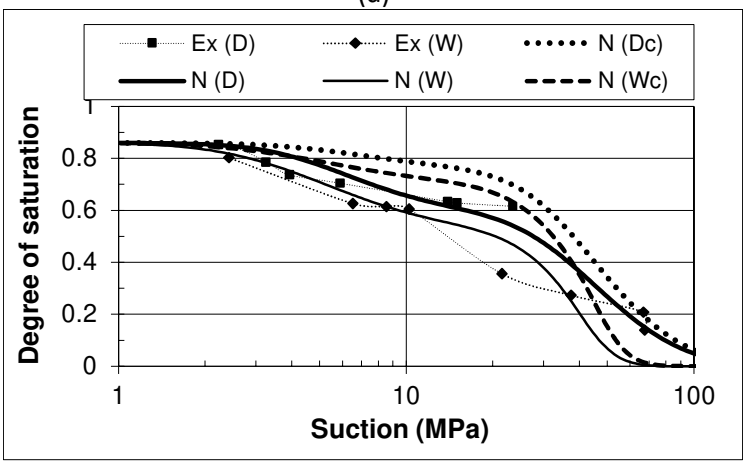
(b)


PSDi
PSDf
NA (Ex)
Relative volume
0.05
0.04
0.03
0.02
0.01
0
0.0001
0.001
0.01
0.1
1
Radius (μm)

(c)




(d)




(e)

**Fig. 10** Experimental (Ex) and numerical (N) (a) GSD, (b) SWRCs, (c) PSD, (d) consolidation tests for Texcoco clay, and (e) shift of the SWRC after first loading. The letter c indicates that the current PSD was used

## CONCLUSIONS

It is proved that the PSD of soils is the main factor affecting the shape of the consolidation curve during primary and secondary consolidation while the influence of viscosity is marginal. Primary consolidation is generated by the flow of water through macrobonds while secondary consolidation is produced by the flow of water through microbonds. When the size distribution of the macro and microstructure shows no overlap, the consolidation curve shows two well-defined steps, one for primary and the other for secondary consolidation. The height and length of the steps for primary

and secondary consolidation depend on the proportion and standard deviation of the macro and microstructure, respectively. The mean size and standard deviation of the macro and microbonds define the position of the step for primary and secondary consolidation in the axis of time, respectively. On the contrary, when the size distributions for macro and microstructure overlap, the consolidation curve shows a single step and it is difficult to differentiate primary from secondary consolidation. When successive loadings are applied to the sample and large deformations are observed, it is convenient to employ the current PSD of the material for the next loading step. The procedure presented in this research allows the simulation of the consolidation curve including both primary and secondary consolidation from the pore size distribution of the soil. Therefore, this procedure shows an important practical application for the computation of the total settlements of structures built on clayey soils as long-term consolidation tests can be waived. More comparisons with experimental data including small load increments and different consolidation times are required to evaluate the precision of the model.

ACKNOWLEDEGEMENTS

The authors would like to thank the following professors and postgraduate students for their help in performing the different laboratory tests: Dra. Damaris Carrales Alvarado, Paulina Sánchez, Rosa Isela Acosta, Bladimir Gutiérrez, Luis García Ledezma and César García.

DECLARATIONS

Author contributions

All authors contributed to the study conception and design. Material preparation, data collection and analysis were performed by Eduardo Rojas, Hiram Arroyo, and Gustavo Gallegos. The first

draft of the manuscript was written by Eduardo Rojas and all authors commented on previous versions of the manuscript. All authors read and approved the final manuscript.

## Credit

Conceptualization: Eduardo Rojas and Hiram Arroyo; Methodology: Eduardo Rojas, Hiram Arroyo and Gustavo Gallegos; Formal analysis and investigation: Eduardo Rojas, Hiram Arroyo and Gustavo Gallegos; Writing - original draft preparation: Eduardo Rojas; Writing Eduardo Rojas, Hiram Arroyo and Gustavo Gallegos; Resources: Gustavo Gallegos; Supervision: Hiram Arroyo and Gustavo Gallegos.

## Funding and competing interests

No funding was received for conducting this study. The authors have no financial or proprietary interests in any material discussed in this article.

## Data availability statement

Data generated or analyzed during this study are available from the corresponding author upon reasonable request.

734 REFERENCES

735

736 Alexandre G, Martins I (2014) An interpretation of secondary consolidation for the Batiscan clay.
737 hal-00940576v2. https://hal.science/hal-00940576v2

738 Alonso EE, Rojas E, Pinyol NM (2008) Suelos parcialmente saturados. In: Proceedings of the *XXIV*
739 Reunión Nacional de Mecánica de Suelos., Aguascalientes, México

740 Andrade MEA (2009) Contribution to the study of soft clays from the city of Santos. MSc. Thesis,
741 COPPE/UFRJ, Rio de Janeiro, Brazil

742 Androutsopoulos GP, Mann R (1979) Evaluation of mercury porosimeter experiments using a
743 network pore structure model. Chem. Engng*. Sc*. 34: 1203-1212.

744 Berre T, Iversen K (1972) Oedometer tests with different specimen heights on a clay exhibiting large
745 secondary compression. Géotechnique 22: 53-70. https://doi.org/10.1680/geot.1972.22.1.53

746 Bjerrum L (1967) Engineering geology of Norwegian normally-consolidated marine clays as related
747 to settlements of buildings. Géotechnique 17: 83-118. https://doi.org/10.1680/geot.1967.17.2.83

748 Chatzis I, Dullien FAL (1977) Modelling pore structure by 2-D and 3-D networks with application to
749 sandstone. J. Can. Pet. Techno*.* 16, 97-108.

750 Cosenza P, Korošak D (2014) Secondary consolidation of clay as an anomalous diffusion process. *Int.*
751 J. Num. Anal. Methods Geomech*.* 38: 1231-1246. https://doi.org/10.1002/nag.2256

752 Crawford CB (1964) Interpretation of the Consolidation Test. J. Soil Mech. Found. Div. 90: 87-102.

753 Christie IF (1964) A re-appraisal of Merchant's contribution to the theory of consolidation.
754 Géotechnique 14: 309-320. https://doi.org/10.1680/geot.1964.14.4.309

755 de Josselin de Jong G (1968) Consolidation models consisting of an assembly of viscous elements or
756 a cavity Channel Network. Géotechnique *18*: 195-228. https://doi.org/10.1680/geot.1968.18.2.195

757 Fatt I (1956) The network model of porous media, I. Capillary pressure characteristics. Trans. Am.
758 Inst. Metall. Pet. Eng*.,* 207, 144-159.
759
760 Figueroa G (1996) La consolidación total unidimensional de los suelos saturados y su aplicación a los
761 hundimientos ocasionados por bombeo. PhD Thesis, UNAM, México.

762 Fleureau JM, Kheirbek-Saoud S, Soemitro R, Taibi S (1993) Behavior of clayey soils in drying-wetting
763 paths. Can. Geotech. J. 30: 287-296. https://dx.doi.org/10.1139/t93-024

764 Gingine V, Cardoso R (2017) Secondary consolidation of a consolidated kaolin slurry during
765 electrokinetic treatment. Engng. Geology 220: 31-42.
766 https://doi.org/10.1016/j.enggeo.2017.01.024

767 Hansen B (1969) A mathematical model for creep phenomena in clay. Special session No. 12.
768 Proceedings of the 7th Int. Conf. Soil Mech. Found. Engng., Mexico City.

769 Liu Y, Borja RI (2022) Time scales in the primary and secondary compression of soils. Int. J. Num.
770 Anal. Methods Geomech. 46: 1383-1408. https://doi.org/10.1002/nag.3350

771 Lo KY (1961) Secondary compression of clays. J. Soil Mech. Found. Div. 87: 61-87.
772 https://doi.org/10.1061/JSFEAQ.0000365

773 Low PF (1979) Nature and properties of water in montmorillonite-water systems. Soil Science Soc.
774 Am. J. 43: 651-658. https://doi.org/10.2136/sssaj1979.03615995004300040005x

775 Martins ISM (1992) Fundamentals of a behavioral model for saturated clayey soils. PhD Thesis,
776 COPPE/UFRJ, Rio de Janeiro Brazil.

777 Martins ISM, Lacerda WA (1985) A theory of consolidation with secondary compression.
778 Proceedings of the 11th Int. Conf. Soil Mech. and Found. Engng., San Francisco, Calfornia. 567-570.

779 Merchant W (1939) Some theoretical considerations on the one-dimensional consolidation of clay.
780 S.M. Thesis, Massachusetts Institute of Technology, Boston.

781 Mesri G, Rokhsar A (1974) Theory of Consolidation for Clays. J. Geotech.l Engng. Div. 100: 567-570.
782 https://doi.org/10.1061/AJGEB6.0000075

783 Rojas E (2022) Towards a Unified Soil Mechanics Theory; The use of effective stresses in unsaturated
784 soils, Bentham Science.

785 Rojas E, Horta J, Arroyo H, López-Lara T, Hernández JB (2024) Fully analytical solution for hydraulic
786 conductivity of soils based on a probabilistic porous model. Int. J. Geomech. 24(4).
787 https://doi.org/10.106/IJGNAI.GMENG-8924

788 Rostami A, Habibagahi G, Ajdan M, Nikooee E (2014) Pore network investigation on hysteresis
789 phenomena and influence of stress state on the SWRC. Int. J. Geomech. 15(5),
790 https://doi.org/10.1061/(ASCE)GM.1943-000315

791 Simms PH, Yanful EK (2001) Measurement and estimation of pore shrinkage and pore distribution
792 in a clayey till during soil–water characteristic curve tests. Can. Geotech. J. 38: 741-754.
793 https://doi.org/10.1139/t01-014

794 Simms PH, Yanful EK (2003) Pore network modelling for unsaturated soils. Proceedings of the 56$^{th}$
795 Canadian Geotechnical Conference , Winnipeg, Manitoba, Canada.

796 Simms PH, Yanful EK (2004) Discussion on the application of mercury intrusion porosimetry for the
797 investigation of soils, including an evaluation of its use to estimate volume change in compacted
798 clayey soils. Géotechnique 54(6): 421-426. https://doi.org/10.1680/geot.2004.54.6.421

799 Wahls HE (1962) Analysis of primary and secondary consolidation. *J. Soil Mech. Found. Div.* 88: 207-
800 231. https://doi.org/10.1061/JSFEAQ.0000463

801 Wu TH, Resendiz D, Neukirchner RJ (1966) Analysis of consolidation by rate process Theory. J. Soil
802 Mech. Found. Div. 92: 229-248. http://doi.org/10.1061/JSFEAQ.0000921.

803 Yang JW, Cui YJ, Mokni N, Ormea E (2024) Investigation into the mercury intrusion porosimetry (MIP)
804 and micro-computed tomography (μCT) methods for determining the pore size distribution of MX80
805 bentonite pellets. Acta Geotech. 19: 85-97. https://doi.org/10.1007/s11440-023-01863-y

806 Yu CY, Chow JK, Wang YH (2016) Pore-size changes and responses of kaolinite with different
807 structures subject to consolidation and shearing. Engng. Geology 202: 122-131.
808 https://doi.org/10.1016/j.enggeo.2016.01.007

809

FIGURE CAPTIONS

**Fig. 1** Consolidation tests at different stresses after Martins (1992)

**Fig. 2** Master curves for different values of parameter $\alpha_H$ and $r$ = 0.25 (after Figueroa 1996)

**Fig. 3** Variation of the viscosity of water with the distance to the solid particle (after Low 1979)

**Fig 4** Pore water pressure profile during a consolidation process

**Fig. 5** The porous model

**Fig. 6** (a) PSD and (b) SWRCs of a Montmorillonite clay

**Fig. 7** Basic units for a) fast and b) slow flow

**Fig. 8** Relative area of pores in a section of soil sample

**Fig. 9** Different cases for the (a) SWRC, (b) the PSD, and (c) consolidation curve of soils

**Fig. 10** Experimental (Ex) and numerical (N) (a) GSD, (b) SWRCs, (c) PSD, and (d) consolidation test for the kaolin sample considering two different viscosities (v) for the adsorbed water layer

**Fig. 11** Experimental (Ex) and numerical (N) (a) GSD, (b) SWRCs, (c) PSD, (d) consolidation tests for Texcoco clay, and (e) shift of the SWRC after first loading. The letter c indicates that the current PSD was used